Cell Reports, Volume *44*

Supplemental information

Computational functions of precisely balanced neuronal microcircuits in an olfactory memory network

Claire Meissner-Bernard, Bethan Jenkins, Peter Rupprecht, Estelle Arn Bouldoires, Friedemann Zenke, Rainer W. Friedrich, and Thomas Frank

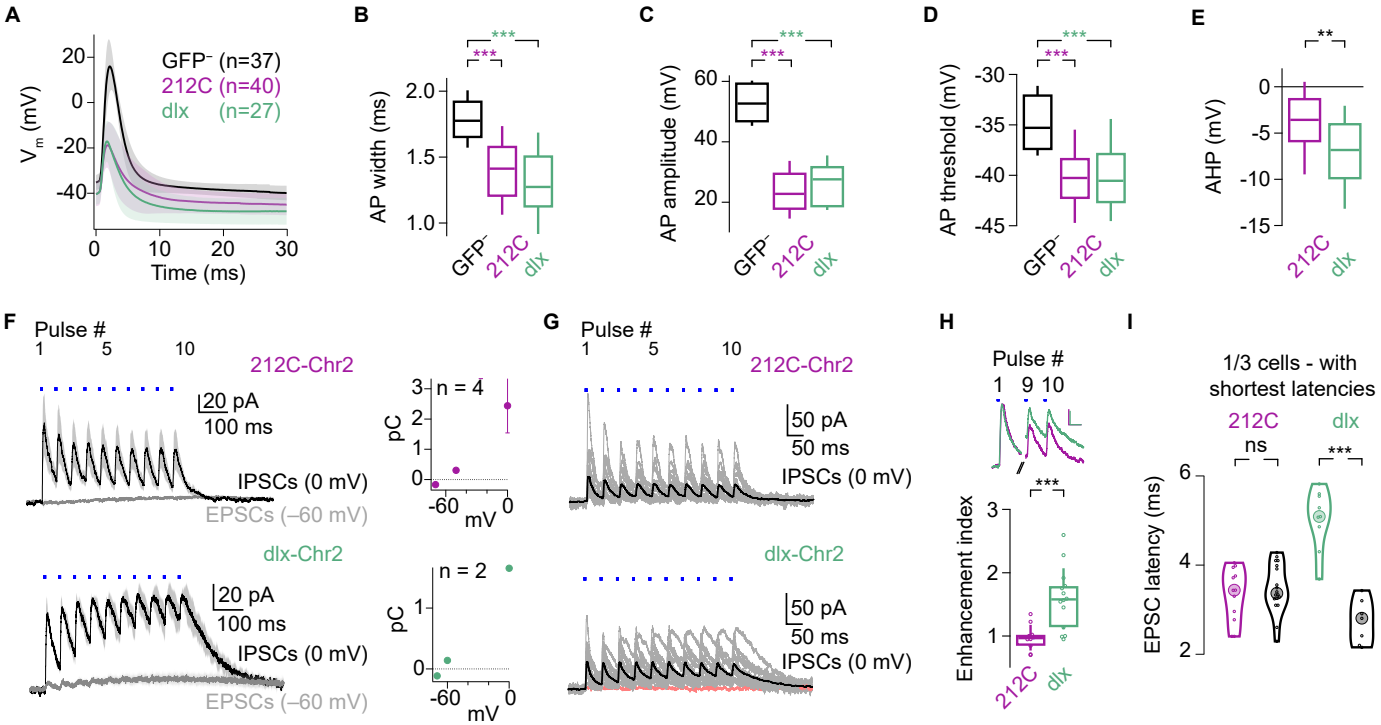

Figure S1 | Further characterization of two populations of inhibitory interneurons in Dp. Related to Figure 1. (A) Mean action potential waveforms (± SD) recorded from 212C-GFP$^+$, dlx:GFP$^+$, and GFP$^-$ neurons (n: number of neurons). **(B)** Comparison of action potential width**,** measured as the time between the two zero crossings of the second derivative of the membrane voltage, before and after the action potential peak, respectively (Kruskal-Wallis test, n = 102, $p < 10^{-9}$). Nonparametric comparisons with GFP$^-$ (n = 37): 212C-GFP$^+$, $p < 10^{-6}$, n = 39; dlx:GFP$^+$, $p < 10^{-7}$, n = 26). In all Fig. S1 box plots, the line represents the median, whiskers show SD, and the box covers the interquartile range. **(C)** Action potential amplitude (Kruskal-Wallis test, n = 102, $p < 10^{-15}$). Nonparametric comparisons with GFP$^-$ (n = 37): 212C-GFP$^+$, Q = 7.56, $p < 10^{-13}$, n = 39; dlx:GFP$^+$, Q = 6.11, $p < 10^{-8}$, n = 26). **(D)** Action potential threshold (Kruskal-Wallis test, n = 103, $p < 10^{-9}$). Nonparametric comparisons with GFP$^-$ (n = 37): 212C-GFP$^+$, $p < 10^{-7}$, n = 39; dlx:GFP$^+$, $p < 10^{-5}$, n = 27). **(E)** Action potential afterhyperpolarization (AHP) amplitude (Wilcoxon rank-sum test: p = 0.009; 212C-GFP$^+$, n = 42; dlx:GFP$^+$, n = 27). **(F)** Left: Mean (± s.e.m.) IPSCs and EPSCs in GFP$^-$ neurons in response to trains (10 pulses at 20 Hz) of 0.5 ms full-field blue light stimulation (blue bars) in 212C-Chr2YFP (top) and dlx-Chr2YFP fish (bottom; same data as in Fig. 1D but showing complete trains). Right: Average (± s.e.m.) charge transfer over the first 50 ms (first "pulse") as a function of holding potential (n: number of neurons). **(G)** IPSCs (gray: individual neurons; black: average) evoked by trains of blue light pulses (0.5 ms) in putative principal neurons in 212C-Chr2YFP (n = 11) and dlx-Chr2 fishYFP (n = 16). Only one neuron (light red trace) showed no IPSCs. **(H)** Top: IPSCs number 1, 9 and 10 evoked by trains of blue light pulses in GFP$^-$ neurons (same as panel G). Bottom: charge transfer evoked by the last two pulses, normalized to the first pulse (Wilcoxon rank-sum test: p = 0.0009; 212C-GFP$^+$, n = 10; dlx:GFP$^+$, n = 14). In dlx-Chr2YFP fish, charge transfer increased because IPSCs broadened. **(I)** Distribution of 33% shortest EPSC latencies in each neuronal population (subset of Fig. 1H data). Short-latency EPSCs were lacking in dlx:GFP$^+$ neurons (Wilcoxon rank-sum test: p = 0.0002; dlx:GFP$^+$, n = 9; dlx:GFP$^-$, n = 7), but not 212C-GFP$^+$ neurons (p = 0.65; 212C-GFP$^+$, n = 12; 212C-GFP$^-$, n = 18). Large circles: median.

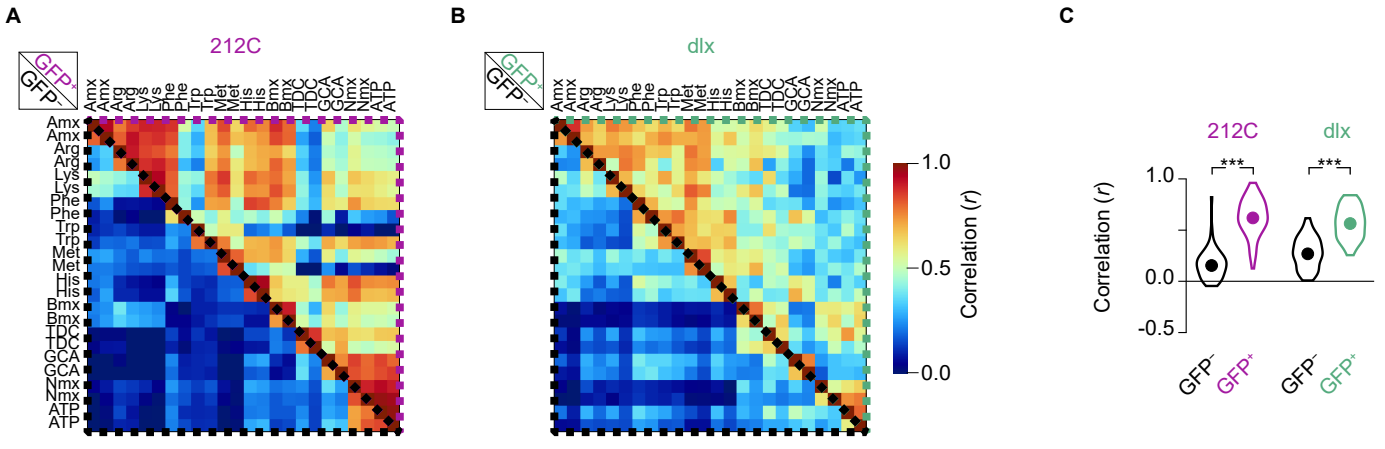

Figure S2 | Population analysis of odor-evoked responses in populations of putative principal cells and interneurons in pDp. Related to Figure 1. (A) Pearson correlation between odor-evoked activity patterns in simultaneously recorded putative principal cells (GFP^- neurons, below diagonal) and interneurons (GFP^+ neurons, above diagonal) in 212C-GFP fish (n = 1515 GFP^- and n = 50 GFP^+ neurons from N = 5 fovs; two trials per odor). **(B)** Same for dlx:GFP fish (n = 1750 GFP^- and n = 65 GFP^+ neurons from N = 12 fovs). **(C)** Distribution of Pearson correlations between all pairwise activity patterns. Two trials with each odor were averaged (Wilcoxon signed rank test; 212C-GFP fish: n = 66 odor pairs, $p < 10^{-19}$; dlx:GFP fish: n = 66 odor pairs, $p < 10^{-16}$). Large circles: median.

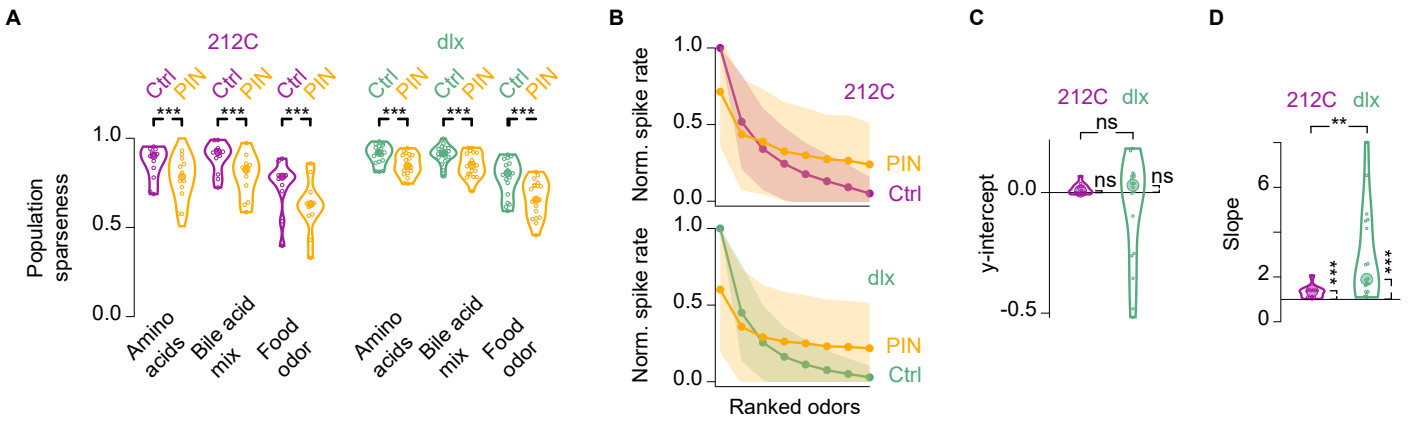

Figure S3 | Effects of PIN on odor- and electrically evoked responses in pDp: additional results. Related to Figure 2. (A) Population sparseness of responses evoked by different classes of odors (amino acids: four individual amino acids and two binary mixtures; bile acids: one 3-component mixtures; one food extract; see Methods for details) under control conditions (Ctrl) and during $vPIN_{212C}$ (left) and $vPIN_{dlx}$ (right). Datapoints represent individual fovs (Wilcoxon signed rank tests: 212C: N = 12 fovs, p = 0.0005 for all three cases: dlx: N = 19 fovs; amino acids: $p < 10^{-4}$; bile acid mix: p = 0.0002; food extract: $p < 10^{-4}$). Large circles: median. **(B)** Rank-ordered odor tuning curves, averaged across neurons (shading: SD). Odor rankings shifted under PIN, as shown by ranking neuronal responses by decreasing amplitude in control conditions and subsequent normalizing, applied consistently across both conditions. **(C)** y-intercepts of linear fits for each fov (Wilcoxon signed rank test against zero median; 212C: p = 0.06, N = 12; dlx: p = 0.78, N = 19; difference between 212C and dlx**;** Wilcoxon rank-sum test: p = 0.69). Large circles: median. **(D)** Slopes of linear fits for each fov (Wilcoxon signed rank test against median of one: 212C: p < 0.001; dlx: p < 0.001; difference between 212C and dlx: p = 0.006). Large circles: median.

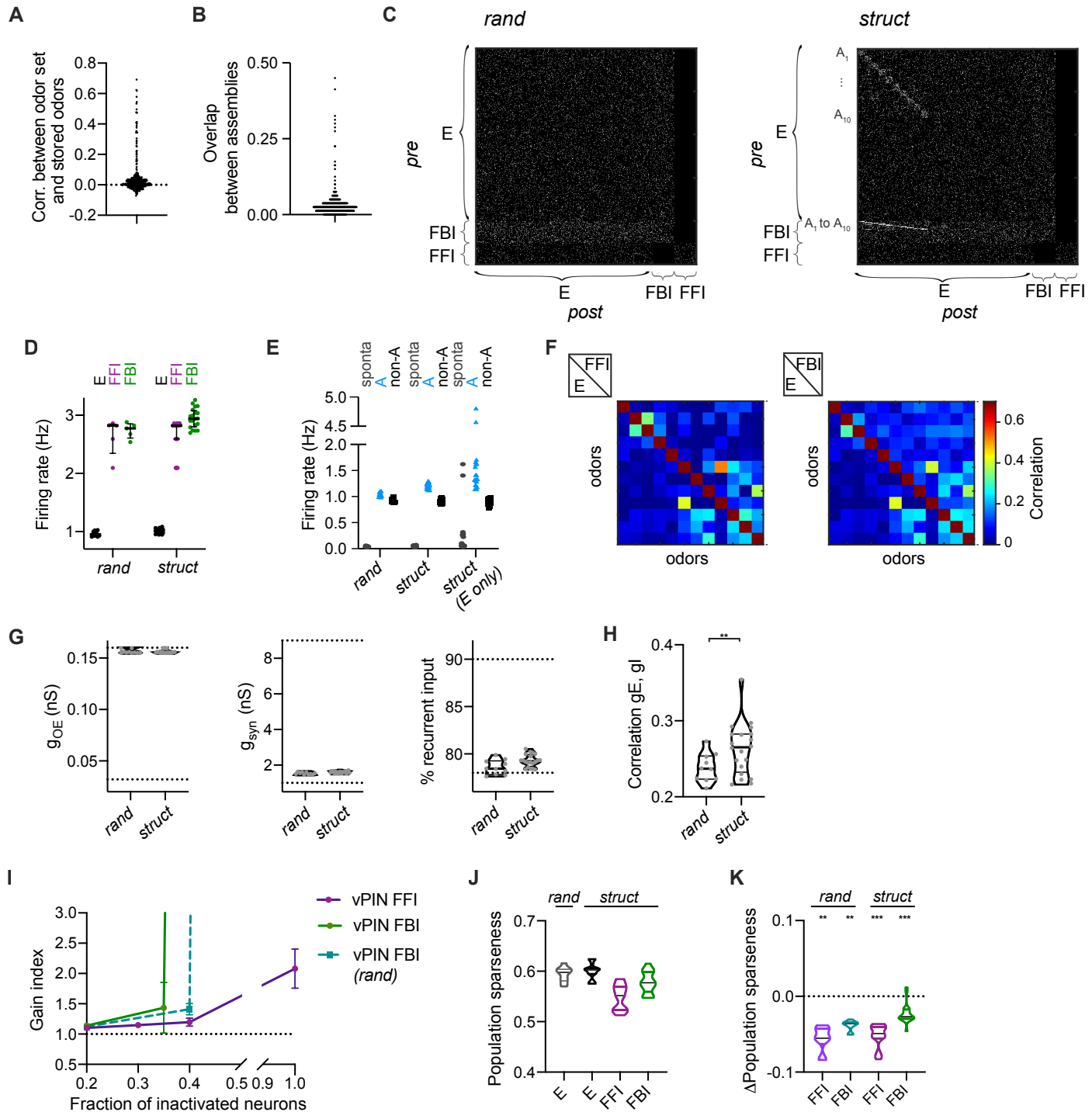

Figure S4 | Computational model of pDp: additional results. Related to Figure 3. (A) Pearson correlation between afferent patterns presented to pDp_{sim} (n = 20) and learned afferent patterns used to create EI assemblies (n = 20). **(B)** Fraction of overlapping neurons between two assemblies. Each data point represents an assembly pair. **(C)** Example connectivity of a *rand* network and a corresponding *struct* network. A white dot indicates the presence of a connection between neurons. Half of the network is depicted, including 10 out of 20 assemblies (A), which consists of 80 E and 10 FBI neurons each. **(D)** Mean firing rates of E, FFI and FBI neurons in *rand* and *struct* networks during presentation of an odor. Each data point represents one network (mean ± SD). **(E)** Firing rates averaged during spontaneous (sponta) activity or during odor presentation, over neurons belonging to an assembly (A) and the remaining ones (non-A). **(F)** Correlations between activity patterns evoked by 12 odors in E (lower triangles) and FFI or FBI (upper triangles). Example of 1 network. **(G)** Left: averaged odor-evoked afferent conductance. Middle: odor-evoked synaptic conductance. Right: percentage of E input coming from recurrent connections during odor presentation. The experimental range measured in *ex-vivo* Dp is delineated by the dotted lines. **(H)** Co-tuning, quantified by the correlation between time-averaged E and I conductances in each neuron in response to various odors (average across neurons, n = 10 and 20 *rand* and *struct* networks, respectively; Wilcoxon matched-pairs signed rank test: p = 0.002). **(I)** Gain index as a function of the fraction of inactivated neurons (mean across networks ± SD). **(J)** Population sparseness of responses evoked by different odors. **(K)** Changes in population sparseness induced by vPIN (vPIN-Ctrl, one sample Wilcoxon signed rank test: FFI, rand: p = 0.002; FBI, rand: p < 0.002; FFI, struct: p < 0.0001; FBI, struct: p < 0.0001).

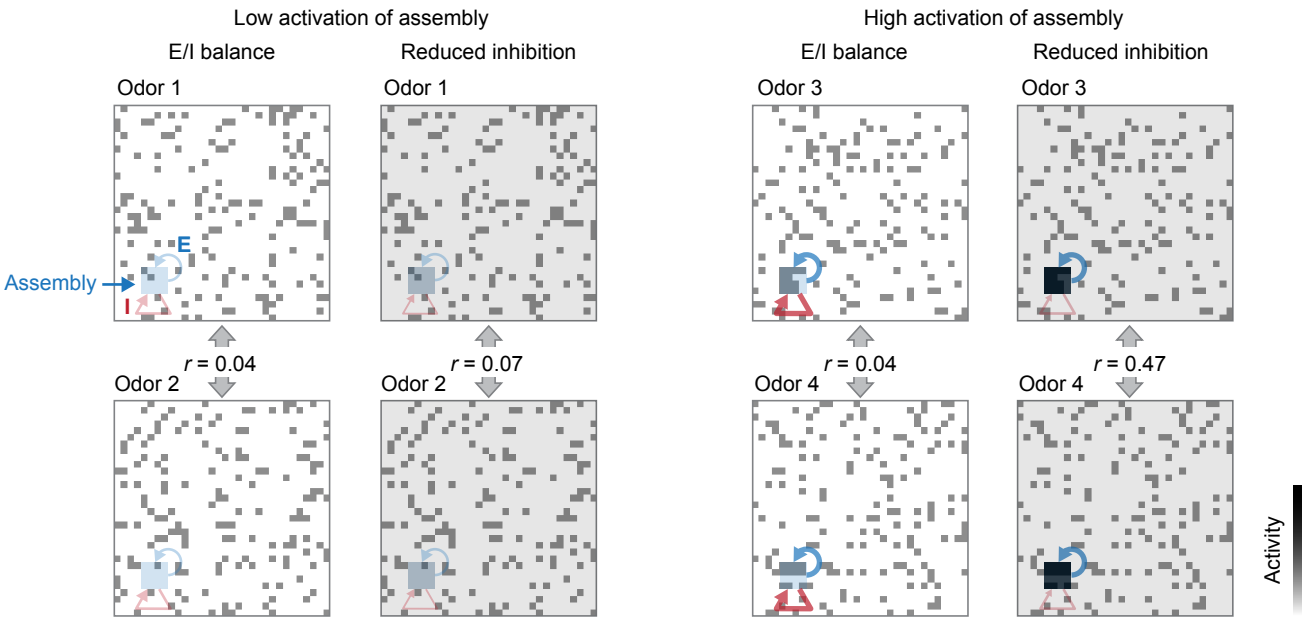

Figure S5 | Mechanism generating runaway correlations: schematic illustration. Related to Figure 4 and 5. Grids represent 32 x 32 E neurons; shaded square depicts an EI assembly; arrows represent feedback excitation (E) and multisynaptic feedback inhibition (I). Left: odors 1 and 2 are uncorrelated and activate a small subset of neurons within the assembly. Reducing inhibition enhances activity within the assembly slightly more than outside the assembly but the resulting increase in pattern correlation remains small. Right: odors 3 and 4 are also globally uncorrelated but activate a larger subset of neurons within the assembly. Because feedback gain increases with assembly activation (non-linear amplification), a reduction in inhibition strongly enhances activity within the assembly. As a consequence, the global pattern correlation becomes high even though activity outside the assembly is uncorrelated. Such "runaway correlation" does not occur when excitation and inhibition are precisely balanced because nonlinear amplification within assemblies is canceled. In poorly balanced networks, runaway correlations therefore emerge in response to subsets of inputs (odors) depending on the precise relation between input patterns (odors) and pre-existing memories (assemblies). Note that this is a schematic illustration with fewer neurons and assemblies than the biologically constrained simulation.

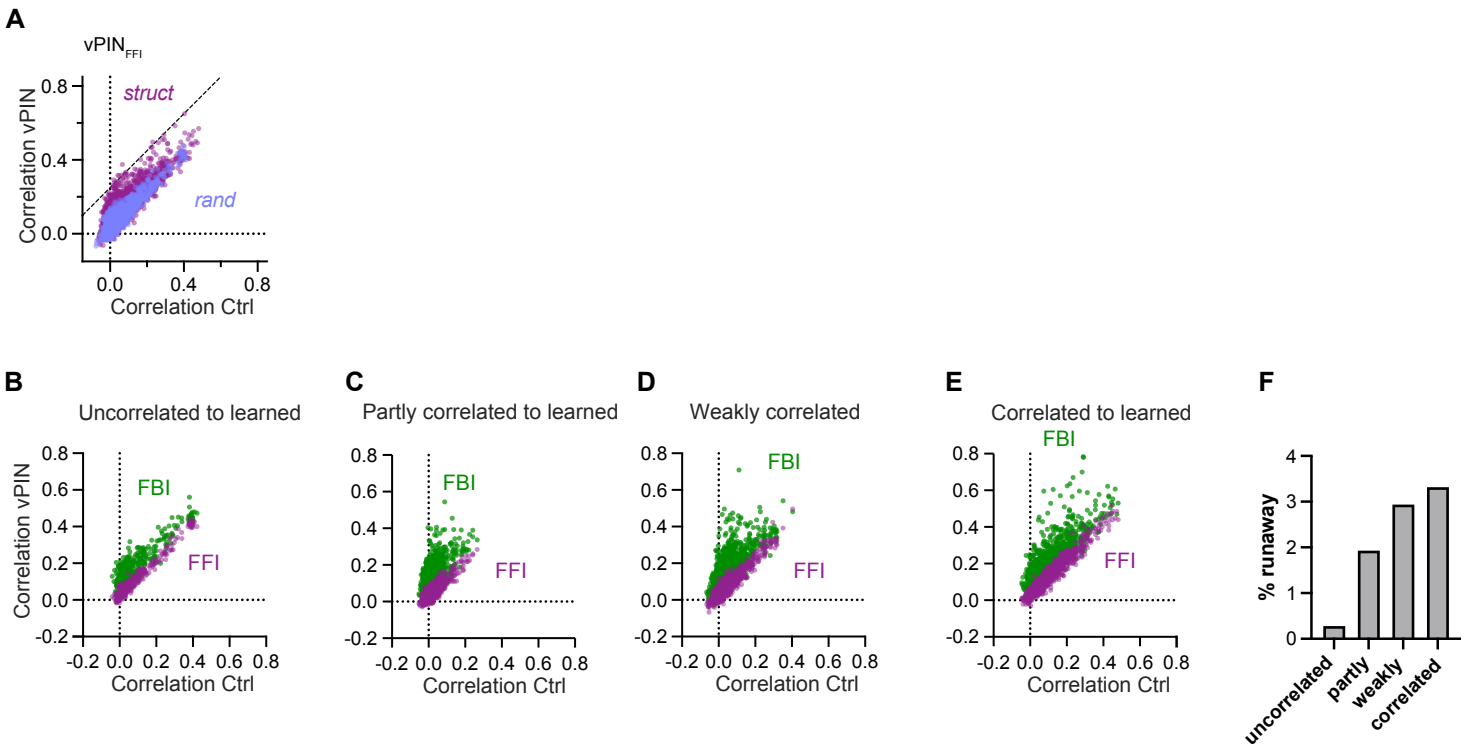

Figure S6 | Additional analysis of runaway correlations. Related to Figure 4. (A) Pattern correlations during vPIN of all FFI neurons as a function of correlations under control conditions (Ctrl) in *rand* and *struct* networks. **(B-F)** The correlations between activity patterns evoked by an odor pair were categorized into four groups based on similarity of the odors to "learned" odors. **(B)** None of the odors in the pair was similar to the 20 "learned" odors (input correlation < 0.1, n = 340 odor pair-network combinations). **(C)** Only one odor in the pair was similar to at least one of the 20 learned odors (correlation > 0.25), while the other was not (correlation < 0.1, n = 1080 odor pair-network combinations). **(D)** Both odors were weakly correlated to the learned odors (0.1 < correlation < 0.25, n = 1390 odor pair-network combinations). **(E)** Both odors in the pair were correlated to at least one of the learned odors (correlation > 0.25, n = 990 odor pair-network combinations). **(F)** Percentage of runaway correlations.

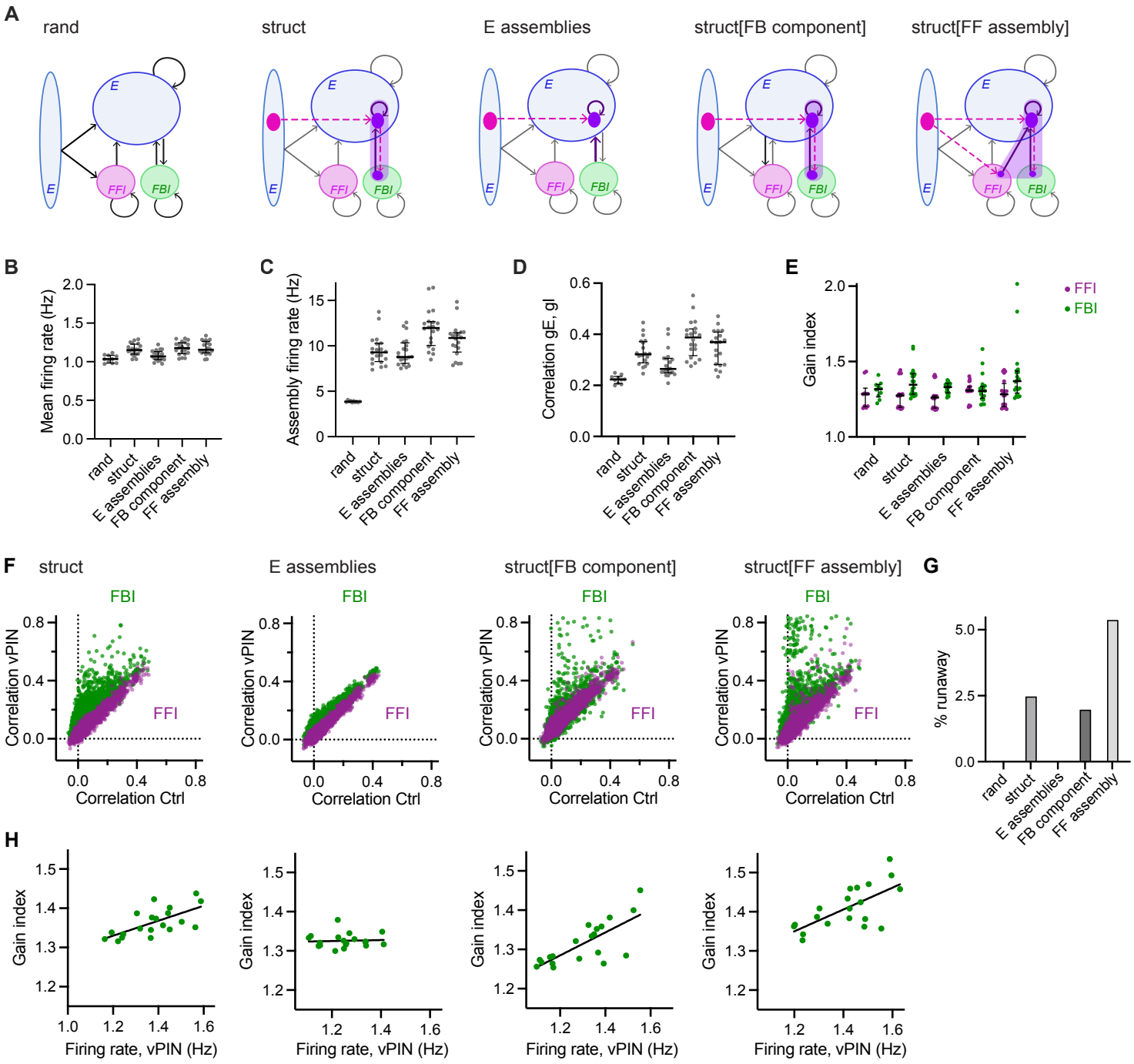

Figure S7 | Model of pDp: variations on connectivity. Related to Figure 4 and 5. (A) Schematics of pDp networks with different connectivity, see associated Supplementary Table 1 for model parameters. From left to right: rand: random networks analyzed in main text; struct: structured networks analyzed in main text (E-I assemblies); E assemblies: networks with E assemblies and global increase of I to E synaptic weights. The connection probability between assembly E neurons was reduced relative to struct networks to align the assemblies' average activity levels (see panel C). struct[FB component]: Since 212C neurons may mediate not only feedforward but also feedback inhibition, we added random feedback inhibitory connections to the FFI population in struct networks. struct[FF assemblies]: E-I assemblies comprise both FFI and FBI neurons. **(B)** Mean firing rates of E neurons during presentation of a learned odor. Each data point in panels (B) through (F) represents one network (n = 20, mean ± SD). **(C)** Mean firing rates of E assembly neurons during presentation of a learned odor. **(D)** Co-tuning, quantified by the correlation between time-averaged E and I conductances in each neuron in response to various odors. **(E)** Gain index. **(F)** Pattern correlations during $vPIN_{FFI}$ and $vPIN_{FBI}$ as a function of correlations under control conditions (Ctrl) in various networks (n = 190 odor pairs, 20 networks). Datapoints above the gray line ($\Delta r > 0.25$) fulfill the operational criterion for runaway correlations. **(G)** Percentage of runaway correlations. **(H)** Gain index as a function of the mean Dp firing rate during vPIN. Each datapoint corresponds to the gain index in response to one odor averaged over 20 networks. Lines are linear fits (E assemblies: $r = 0.065$, p = 0.7865; struct[FB component]: $r = 0.75$, p = 0.0001; struct[FF assembly]: $r = 0.67$, p = 0.0011).

A

	Average connectivity increase
struct and struct[FB component]	$p_{E\text{-}E}$(assembly): 5 $p_{I\text{-}E}$(assembly): 9.5
E assemblies	$p_{E\text{-}E}$(assembly): 3.5 $w_{FBI,E}$(all): 1.04
struct[FF assembly]	$p_{E\text{-}E}$(assembly): 5 $p_{FBI\text{-}E}$(assembly): 9.5 $p_{FFI\text{-}E}$(assembly): 12.5

B

struct[FB component]

Connectivity	Synaptic strengths w_{YX} (pS)
OB → E*	130-134
OB → I_{ff}	16-19
E → E*	100
E → I*	56-70
I → E	380-450
I → I	380-440

Supplementary Table 1: Model parameters related to Supplementary Figure 7.
A. Connectivity within assemblies ($p_{pre\text{-}post;}$ $w_{pre,post}$). The value indicates the fold increase in probability between assembly neurons compared to the probability among neurons outside assemblies. In *struct[FF assembly]* networks, the assembly size was similar to that of *struct* networks, except half of the inhibitory assembly neurons were FBI while the other half were FFI. B. Adjusted synaptic strengths in *struct[FB component]* networks ($p_{E\text{-}I_{ff}}$ = 0.02). The asterisk denotes unchanged parameters.